Modulation of homogeneous and isotropic turbulence by sub-Kolmogorov particles: Impact of particle field heterogeneity

Roxane Letournel, Frédérique Laurent, Marc Massot, Aymeric Vié

Modulation of homogeneous and isotropic turbulence by sub-Kolmogorov particles: impact of particle field heterogeneity

Roxane Letournel[a,b,c,*], Frédérique Laurent[a,b], Marc Massot[c], Aymeric Vié[a,b]

[a] *Laboratoire EM2C UPR 288, CNRS, CentraleSupélec, Université Paris-Saclay, 3, rue Joliot-Curie 91192 Gif-sur-Yvette cedex France*
[b] *Fédération de Mathématiques de CentraleSupélec, CNRS, 3, rue Joliot-Curie 91192 Gif-sur-Yvette cedex France*
[c] *Centre de Mathématiques Appliquées, CNRS, Ecole polytechnique, Institut Polytechnique de Paris, Route de Saclay, 91128 Palaiseau Cedex, France*

Abstract

The modulation of turbulence by sub-Kolmogorov particles has been thoroughly characterized in the literature, showing either enhancement or reduction of kinetic energy at small or large scale depending on the Stokes number and the mass loading. However, the impact of a third parameter, the number density of particles, has not been independently investigated. In the present work, we perform direct numerical simulations of decaying Homogeneous Isotropic Turbulence loaded with monodisperse sub-Kolmogorov particles, varying independently the Stokes number, the mass loading and the number density of particles. Like previous investigators, crossover and modulations of the fluid energy spectra are observed consistently with the change in Stokes number and mass loading. Additionally, DNS results show a clear impact of the particle number density, promoting the energy at small scales while reducing the energy at large scales. For high particle number density, the turbulence statistics and spectra become insensitive to the increase of this parameter, presenting a two-way asymptotic behavior. Our investigation identifies the energy transfer mechanisms, and highlights the differences between the influence of a highly concentrated disperse phase (high particle number density, limit behavior) and that of heterogeneous concentration fields

*Corresponding author
Email address: roxane.letournel@centralesupelec.fr (Roxane Letournel)

(low particle number density). In particular, a measure of this heterogeneity is proposed and discussed which allows to identify specific regimes in the evolution of turbulence statistics and spectra.
Keywords: Particle dynamics, homogeneous isotropic turbulence, two-way coupling, heterogeneity.

Introduction

Turbulent flows laden with particles or droplets are common in many engineering and environmental applications, such as atmospheric dispersal of pollutants, liquid sprays in engines, sediments in rivers, droplets in clouds etc. The turbulence can completely govern the particles' behavior, and in the case of flows with a high disperse phase mass loading, the presence of particles can also influence the turbulence (Squires and Eaton, 1990; Boivin et al., 1998).

In the literature, the interactions between a turbulent carrier phase and a particulate phase in the point-particle limit have been extensively studied. In the one-way coupled context, for which the particles do not affect the carrier phase, the importance of Stokes number based on Kolmogorov or Lagrangian integral time scales have been demonstrated: the former characterizes the occurence of preferential concentration (Eaton and Fessler, 1994) while the latter is representative of the transition to particle-trajectory-crossing dominated flows (Février et al., 2005).

In the case of two-way coupling, turbulence modulation by particles has been also investigated in Homogeneous Isotropic Turbulence (HIT), focusing on the effect of the Stokes number and mass loading. On the one hand, studies on stationary HIT of Squires and Eaton (1990); Boivin et al. (1998); Mallouppas et al. (2017) showed that the turbulent kinetic energy of the carrier phase is reduced by particles. They concluded that inertial particles inject energy in the turbulent motion at high wavenumbers with a corresponding increase in the dissipation, which was also described by Squires and Eaton (1994) with respect to mass loading.

On the other hand, Elghobashi et al. (1994); Druzhinin and Elghobashi (1999);

Druzhinin (2001); Ferrante and Elghobashi (2003); Abdelsamie and Lee (2012) worked with a decaying HIT and found that particles with low Stokes number can slow the decay of fluid energy. Indeed, studies on the fluid-particle interaction spectrum reveal a negative contribution at low wave numbers where intensity is reduced when Stokes number increases, whereas the energy rate at large wavenumbers remains positive. More generally, Ferrante and Elghobashi (2003) classified particles according to their Stokes number and described the evolution of turbulent energy and dissipation of the flow, and Sundaram and Collins (1999) showed that the shift in energy to high wavenumbers in the fluid phase increases the viscous dissipation rate. The focus of all these studies was the influence of the Stokes number and mass loading: the former parameter globally determines the dynamics of particles in a given fluid and the latter plays a role in the inverse-coupling force that the particles exert on the fluid. Table 1 summarizes some of the previous works, and the parameters studied.

A dimensional analysis leads to the identification of a third controlling parameter, the particle number density. In fact, this parameter plays a key-role: for high number density, the proximity of particles can lead to a continuous phase behavior, while for low number density, distant particles can produce strong local effects on the surrounding fluid and the exact location of the particles may have a great impact on the dynamics of the flow, depending on the realization. In the literature, this parameter has been first studied in the objective of reaching statistical convergence for one-way coupled simulations (Vié et al., 2016). Strutt et al. (2011) observed the lack of consensus regarding the number of particles that must be considered in simulations. A common definition for statistical convergence is the point at which the particle dispersion statistics do not change significantly (i.e. become independent on the number of particles). On the other hand, Sundaram and Collins (1999) studied a regime with very low particle number density, for which each particle acts independently and observed that their collective effect on the fluid scales linearly with the total number of particles.

In the present work, we investigate the effect of the particle number density along with the mass loading and the Stokes number. We propose a characterization and a measure for the heterogeneity of the particulate phase. We identify two regimes in

Reference	**Forcing**	$\mathbf{M_r/M_c}$	**Fixed**	**Changed**
Squires and Eaton (1990)	YES	100	St, n_η	$\boldsymbol{\phi}$, α, ρ_p/ρ_f, d_p/η
Elghobashi et al. (1994)	NO	100	α, St	$\boldsymbol{d_p/\eta}$, ρ_p/ρ_f, n_η , ϕ
			α, d_p/η, n_η	$\mathbf{St}$, ρ_p/ρ_f, ϕ
			St, ρ_p/ρ_f, d_p/η	$\boldsymbol{\alpha}$, ϕ, n_η
Squires and Eaton (1994)	YES	1	St, n_η	$\boldsymbol{\phi}$, α, ρ_p/ρ_f, d_p/η
Boivin et al. (1998)	YES	> 1	α, ϕ, ρ_p/ρ_f	$\mathbf{St}$, d_p/η, n_η
			St, n_η	$\boldsymbol{\phi}$, ρ_p/ρ_f, α, d_p/η
Druzhinin and Elghobashi (1999)	NO	1	St, ρ_p/ρ_f, d_p/η	$\boldsymbol{\phi}$, α, n_η
Sundaram and Collins (1999)	NO	1	α, ϕ, ρ_p/ρ_f	$\mathbf{St}$, d_p/η, n_η
			St, d_p/η, ρ_p/ρ_f	$\boldsymbol{\alpha}$, ϕ, n_η
Druzhinin (2001)	NO	1	α, ϕ, ρ_p/ρ_f	$\mathbf{St}$, d_p/η, n_η
Ferrante and Elghobashi (2003)	NO	47	α, ϕ, ρ_p/ρ_f	$\mathbf{St}$, d_p/η, n_η
Abdelsamie and Lee (2012)	YES vs NO	95	α, ϕ, ρ_p/ρ_f	$\mathbf{St}$, d_p/η, n_η
Mallouppas et al. (2017)	YES	1	α, d_p/η, n_η	$\mathbf{St}$, ρ_p/ρ_f, ϕ
			St, ρ_p/ρ_f, d_p/η	$\boldsymbol{\phi}$, α, n_η

Table 1: Previous studies of the modulation of turbulence by disperse phase. Forcing scheme for stationary HIT and ratio of real particles per computational particle are specified for each study. Choice of fixed parameters and studied parameters are displayed in the two last columns. In the table, St is the Stokes number, α is the volume fraction, n_η is the particle number density, ϕ is the mass fraction, ρ_p/ρ_f is the ratio of particle and fluid densities and d_p/η is the ratio of particle's diameter and Kolmogorov scale. $\mathbf{M_r/M_c}$ is the ratio of the number of real particles per computational particle.

two-way coupled flows, according to the level of heterogeneity of the disperse phase: an asymptotic behavior for highly-concentrated particle phase (high particle number density), and a strong response of turbulence at small scales for the heterogeneous particle phase. We provide some characterization of turbulence statistics and energy spectra for those specific regimes and explain the transition between them for intermediary particle number densities.

In section 1, we first present the assumptions and governing equations of our study, as well as the numerical methods. Then, the target HIT configuration and the parameter set are presented in section 2, with an emphasis on the other parametric studies in the literature. A definition of heterogeneity is detailed in section 3 along with the way to measure it unequivocally when preferential concentration occurs. Results of the extensive study are presented in section 4, in the following order: turbulence modulation by particles is measured through the analysis of global energy transfers (section 4.1). Then, deeper insight is given by an analysis in the spectral domain (section 4.2), permitting to identify specific regimes with respect to the number density of the particulate phase. These regimes are further analyzed in section 4.3, in particular with regard to coupling mechanisms.

1. Modeling and numerical frameworks

1.1. Fluid and particles equations

We consider monodisperse solid spherical particles of fixed size. Particles diameter is smaller than the Kolmogorov length scale ($d_p << \eta$), thus particle-resolved DNS is not necessary (Fröhlich et al., 2018), and a point-particle approximation is adopted. The density ratio between the particles and the fluid is large ($\rho_p >> \rho_f$) and the Reynolds number of the particle is smaller than one ($Re_p \leq 1$). The volume fraction α is small enough to consider particle-particle collisions as negligible (dilute regime: $\alpha < 10^{-3}$). Therefore, many of the forces in the original Basset-Boussinesq-Oseen equation are assumed negligible compared to the drag force. Furthermore, if the drag force obeys Stokes' law, the equation of motion is linear in the velocity difference

between fluid and particle. Then the motion equations of particles are written as

$$\begin{cases} \dfrac{d\mathbf{x}_p(t)}{dt} &= \mathbf{v}_p(t) \\ \dfrac{d\mathbf{v}_p(t)}{dt} &= \dfrac{\mathbf{u}_{f@p}(t) - \mathbf{v}_p(t)}{\tau_p} \end{cases} \tag{1}$$

where $\mathbf{x}_p(t)$ and $\mathbf{v}_p(t)$ stand for particle position and velocity at time t, and $\mathbf{u}_{f@p}(t) = \mathbf{u}_f(t, \mathbf{x}_p(t))$ is the undisturbed fluid velocity evaluated at the particle position. The particle relaxation time τ_p is defined as $\tau_p = \dfrac{\rho_p d_p^2}{18\mu_f}$ where μ_f is the dynamic viscosity of the fluid. The effects of particles on the carrier phase are expressed through an additional force in the momentum equation of the fluid. For an incompressible fluid, the equations of motion for the carrier fluid are:

$$\begin{cases} \dfrac{\partial u_{f,i}}{\partial x_i} &= 0 \\ \dfrac{\partial u_{f,i}}{\partial t} + \dfrac{\partial u_{f,i}u_{f,j}}{\partial x_j} &= \dfrac{-1}{\rho_f}\dfrac{\partial P}{\partial x_i} + \dfrac{\mu_f}{\rho_f}\dfrac{\partial^2 u_{f,i}}{\partial x_j \partial x_j} + \dfrac{1}{\rho_f} f_i \end{cases} \tag{2}$$

where $\mathbf{f}$ is the force exerted by particles on the fluid.

1.2. Coupling equations

A projection kernel Δ is introduced to give a local average of the feedback force. This function is positive, monotically decreasing and normalized such that its integral over the entire physical space is unity. The source term $\mathbf{f}$ in Eq.2 is then written as:

$$\mathbf{f}(\mathbf{x}, t) = \sum_p \mathbf{F}^{(p)} \Delta(\mathbf{x} - \mathbf{x}_p(t)) \tag{3}$$

where $\mathbf{F}^{(p)} = m_p \frac{\mathbf{v}_p(t) - \mathbf{u}_{f@p}(t)}{\tau_p}$ is the resultant force exerted by a particle p of mass m_p on the fluid.

Other Eulerian spatial fields can therefore be defined as:

$$n(\mathbf{x}, t) = \sum_p \Delta(\mathbf{x} - \mathbf{x}_p(t)) \tag{4}$$

$$n(\mathbf{x}, t)\tilde{\mathbf{v}}_p(\mathbf{x}, t) = \sum_p \mathbf{v}_p \Delta(\mathbf{x} - \mathbf{x}_p(t)) \tag{5}$$

$$n(\mathbf{x}, t)\tilde{\mathbf{u}}_{f@p}(\mathbf{x}, t) = \sum_p \mathbf{u}_{f@p} \Delta(\mathbf{x} - \mathbf{x}_p(t)) \tag{6}$$

Spatial averages can then be derived and the notation used is $\langle f(\mathbf{x},t)\rangle = \frac{1}{|\mathcal{V}_f|}\int_{\mathcal{V}_f} f(\mathbf{x},t)d\mathbf{x}$, where $\mathcal{V}_f$ indicates that the integral is taken over the whole domain of fluid $|\mathcal{V}_f| = L^3$. For monodisperse spherical particles, $m_p = \rho_p \pi d_p^3/6$ and global volume fraction is defined as $\alpha = n_0 \pi d_p^3/6$, where n_0 is the mean particle number density $\langle n(\mathbf{x},t)\rangle = n_0$. The mass loading of the disperse phase is therefore defined as $\phi = \alpha\rho_p/\rho_f$. To highlight the effect of these parameters, the coupling term is expressed as:

$$\frac{1}{\rho_f}\mathbf{f}(\mathbf{x},t) = \phi\frac{n(\mathbf{x},t)}{n_0}\frac{\tilde{\mathbf{v}}_p(\mathbf{x},t) - \tilde{\mathbf{u}}_{f@p}(\mathbf{x},t)}{\tau_p} \tag{7}$$

The mass fraction term is thus a factor in the expression, the fraction $n(\mathbf{x},t)/n_0$ contains information about the spatial distribution of particles and the last term is related to the Stokes number.

1.3. Numerical methods

We performed direct numerical simulation to solve the unsteady three-dimensional Navier-Stokes and continuity equations with the Asphodele code using a low Mach formulation of the Navier-Stokes equations and a Lagrangian formulation for the particles. This code was developed by J. Réveillon and co-workers at CORIA laboratory (Reveillon and Demoulin, 2007). The time resolution is provided by a third order explicit Runge Kutta scheme and spatial evolution is done with a finite difference scheme, the derivatives being computed with a Pade 6th order scheme (Lele, 1992).

One of the key aspects of in Euler-Lagrange simulation is the coupling between the particle equations and the carrier phase. Two elements are required: an interpolation scheme to evaluate the gas phase properties at the particle locations, and a projection scheme to compute the feedback of particles to the gas phase or to compute particle Eulerian fields.

For the interpolation step, the Asphodele solver uses a second-order trilinear algorithm to compute the carrier phase quantities at droplet location. Strutt et al. (2011) discussed the accuracy of interpolation schemes such as the fourth-order cubic spline, the fifth-order Lagrange or the third-order Hermite polynomials interpolation and they concluded that the three schemes gave similar mean square particle displacements, advising to use the least computationally expensive Hermite polynomials interpolation.

Moreover, a recent work has also shown that a lower-order interpolation combined with uncorrected fluid velocity could lead to an improved drag estimation (Horwitz and Mani, 2016). Regarding these works, the choice of a second-order algorithm seems to be a reasonable solution with respect to the up-to-date literature.

The choice of the projection kernel depends on the particles properties and the desired precision. The PSI-Cell method of Crowe et al. (1977) was originally implemented in Asphodele code. The Lagrangian contributions are instantaneously allocated to neighboring gas nodes, weighted by the distance to the nodes. This procedure is sometimes controversial because it leads to significant error that depends on the ratio of particle diameter to the grid spacing. This approach requires for the mesh size to be much larger than the particle diameter, as demonstrated by Capecelatro et al. (2015); Horwitz and Mani (2016); Ireland and Desjardins (2017); Balachandar et al. (2019). Various mollification kernels can be used to transfer particle data on the Eulerian mesh, depending on the quantity of interest. Some of them are described by Capecelatro and Desjardins (2013). Diffusion operation might also be necessary to deal with finer grids (Poustis et al., 2019). Maxey et al. (1997) proposed a "narrow envelope function" in the form $\Delta(\mathbf{x}) = (2\pi\sigma^2)^{-3/2}\exp(-\mathbf{x}^2/2\sigma^2)$, which was used by other works (Capecelatro and Desjardins, 2013; Zamansky et al., 2014). The length scale σ is a parameter that can be adjusted to reflect the finite size of the particle. A gaussian envelope for the source term was also implemented in the code and a comparison of the influence of the projection kernels is provided in Appendix A: the effect of the coupling kernel is limited to the smallest scales and does not impact the qualitative results that are reported in this work.

Another concern discussed in literature is about recovering the undisturbed velocity of the fluid at particle position. This was extensively studied by Gualtieri et al. (2015); Horwitz and Mani (2016); Ireland and Desjardins (2017); Balachandar et al. (2019); Zamansky (2019) who have developed models to estimate this quantity in two-way coupled problems. Based on their results, given the ratio of particle diameter with grid spacing of our simulations ($d_p << \Delta x$), we do not require this level of modeling and the conclusions of our work are expected not to be affected by such a choice.

2. Target configuration and parameter sets

2.1. Homogeneous Isotropic Turbulence

Among the works mentioned in the introduction, we can distinguish studies with forced stationary turbulence, for which statistics are therefore easier to carry out, from naturally decreasing turbulences, as reported in the first column of Table 1. A comparison of these turbulences is proposed by Abdelsamie and Lee (2012), who noted a number of difficulties in the attempt to study the impact of particles on the energy spectrum when it is artificially forced. Many differences are observed, including significant changes in the influence of small particles that do not allow energy to be reintroduced to the fluid in forced turbulence. And although Mallouppas et al. (2013) introduced a new forcing model, the same biases observed for small particles are found in their results. We have therefore chosen a configuration of decaying turbulence, for which we normalize the observed quantities by the total kinetic energy at each instant and thus retrieve more stationary trends in the evolution of components of the energy decay rate.

The proposed test case is a decaying homogeneous isotropic turbulence loaded with particles. The domain is a cubic periodic box of size $L = 5$ meshed with $N_g^3 = 256^3$ cubic cells. The initial condition for the carrier phase is set using a Pope spectrum (Pope, 2000). The initial parameters of the spectrum are $C = 1.5$, $\beta = 5.2$ and $p_0 = 4$, $c_L = 0.019$, $c_\eta = 0.051$. All the values of the variables presented in this work are dimensionless and the normalizing Reynolds number is $\mathrm{Re} = u_{ref} L_{ref}/\nu_f = 10^3$. The reference velocity u_{ref} and length L_{ref} based on the macroscopic characteristics of the computational domain allow to define a reference time scale for the carrier phase: $t_{ref} = L_{ref}/u_{ref}$. We provide dimensional quantities for illustration purposes, based on an estimated velocity of $u_{ref} = 1$m/s and $L_{ref} = 1$m.

Adequate resolution of statistics is verified with the parameter $\kappa_{max}\eta = 2\pi/L \times N_g/2\eta = 2.9 \geq 1$. We verified the convergence of the spectra for different grid sizes in Fig. 1(a). Spectra overlapped in their definition domain, which ensures that the smallest scales are always appropriately resolved. The results presented in this work were obtained using the 256^3 grid. The turbulent characteristics of the decaying HIT are given

time	e	ε	τ_k	η	τ_f	L_{11}	Re_L	Re_λ
t_0	0.015	0.0089	0.335	0.018	2.11	0.21	21.13	15.9
$t_{inj} = 3$	0.054	0.0014	0.854	0.029	4.55	0.27	16.45	14.6
$t_f = 6$	0.003	0.00052	1.38	0.037	6.95	0.31	13.47	12.7

Table 2: Turbulence properties of the HIT

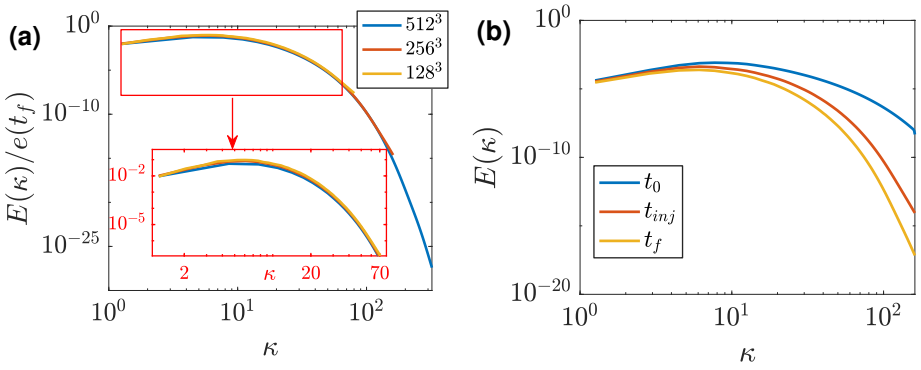

Figure 1: (a) Comparison of the normalized Energy spectrum for different size of meshgrids. The inset displays a zoom around the largest scales. (b) Energy spectra at initial time, injection time and final time.

in Table 2 for initial time, injection time and final time. It shows the mean turbulent kinetic energy e, the dissipation ε , the Kolmogorov time and length scales (τ_k and η), the Eulerian eddy turn-over time τ_f , the longitudinal integral length scale L_{11}, and the turbulent Reynolds number based on the integral length scales $\mathrm{Re}_L = u_{rms} L_{11}/\nu_f$, where $u_{rms} = \sqrt{2/3e}$ is the gas velocity fluctuations. The energy spectrum is plotted for the corresponding times in Fig. 1(b).

To evaluate turbulence modulation by particles, statistical quantities and spectrum of energy are studied. The fluid energy equation is obtained by multiplying fluid momentum equation by $u_{f,j}$ and ensemble averaging.

$$\frac{de(t)}{dt} = -\varepsilon(t) + \psi_p(t) \tag{8}$$

where $\varepsilon(t) = 2\nu_f \langle S_{ij} S_{ij} \rangle$ is the viscous dissipation rate of $e(t)$ with $S_{ij} = \frac{1}{2}\Big(\frac{\partial u_{f,i}}{\partial x_j} + \frac{\partial u_{f,j}}{\partial x_i}\Big)$ and ν_f is the dimensionless kinematic viscosity. $\psi_p(t)$ represents the energy

rate of change due to the particles drag force:

$$\psi_p(t) = \frac{\phi}{\tau_p n_0}\Big\langle n(\mathbf{x},t)u_{f,i}(\mathbf{x},t)[\tilde{v}_{p,i}(\mathbf{x},t) - \tilde{u}_{f@p,i}(\mathbf{x},t)]\Big\rangle \tag{9}$$

The homogeneous isotropic field allows us to use the spatial mean $\langle . \rangle$ previously introduced instead of the ensemble averaging. It is numerically implemented as the discrete average over all the cells in the domain.

Performing the Fourier transform of the fluid momentum equation, we obtain the equation for the energy spectrum $E(\kappa)$:

$$\frac{\partial E(\kappa,t)}{\partial t} = T(\kappa,t) - D(\kappa,t) + \Psi_p(\kappa,t) \tag{10}$$

where the spectral dissipation rate is $D(\kappa) = 2\nu_f\kappa^2 E(\kappa)$ and $T(\kappa)$ is the spectral energy transfer rate. The fluid-particle energy interaction term $\Psi_p(\kappa)$ produced by particles is responsible for the modulation in the turbulence energy spectrum. It is defined by:

$$\Psi_p(\kappa,t) = -\sum_{\kappa\leq|\boldsymbol{\kappa}|\leq\kappa+1} \Re\Big\{\hat{u}^{\star}_{f,i}(\boldsymbol{\kappa})\frac{\hat{f}_i(\boldsymbol{\kappa})}{\rho_f}\Big\} \tag{11}$$

where "$\hat{}$" denotes Fourier transform, "$\star$" the complex conjugate, and $\Re\{\}$ denotes the real part.

2.2. Key-parameters and dimensional analysis

Particles are injected at $t = 1$, with particles' location randomly sampled according to a uniform distribution law in the domain, and the particle velocities are set equal to the ones of gas phase at the particle locations. Natural turbulence has established at that time: the relation $\partial e/\partial t = -\varepsilon(t)$ is satisfied. The simulation is run under one-way coupling during approximately one eddy turn over time to thermalize the particles. Then the two-way coupling is activated at $t_{inj} = 3$. This delay for the activation of the two-way coupling allows the influence of the particles to be studied once they have naturally segregated. This removes an inconvenient transitional regime observed otherwise, already mentioned by Ferrante and Elghobashi (2003), especially visible for particles with large Stokes number.

Regarding some properties of the turbulent flow, dimensionless numbers can be derived, considering fluid density ρ_f, Kolmogorov time $\tau_k = \left(\nu_f/\varepsilon\right)^{1/2}$ and length scale $\eta = \left(\nu_f^3/\varepsilon\right)^{1/4}$. This yields the ratio of the characteristic time of a particle and a turbulence time scale, commonly referred to as the Stokes number $\mathrm{St} = \tau_p/\tau_k$, the ratio of the diameter of particles and Kolmogorov length scale d_p/η and the dimensionless particle number density, introduced by Poelma et al. (2007), noted $n_\eta = n_0\eta^3$, that can be interpreted as the number of particles per Kolmogorov eddy. Volume fraction α, mass loading ϕ and density ratio can also be derived. All those parameters are related to each other in Fig. 2.

The dispersed phase is completely defined with three parameters : particle diameter, particle density and mean particle number density. The carrier phase is more complex. Physical parameters are fluid density ρ_f and fluid viscosity μ_f, but a number of scales and other characteristics are required to completely define turbulence. Actually, the entire initial energy spectrum should be taken into consideration. However, because the Reynolds number is small enough and there is therefore no scales separation, turbulence can be essentially characterized by the smallest scales η and their characteristic time τ_k (which is equivalent to giving their energy level). Note that by considering more parameters to characterize turbulence, other dimensionless numbers can be introduced (based on integral length scales for example). According to the Pi-theorem, the problem with seven parameters expressed in three fundamental units (mass, length, time) can thus be expressed with four dimensionless numbers. Three of them combine the parameters of the two phases such as the dark ones in Fig. 2 and the last one only characterizes the carrier phase: in our case it is the Reynolds number based on the smallest scales.

The reader can re-examine previous publications with this diagram in mind. Table 1 shows the parameters that were fixed and changed between their different simulations. The parameters in bold font were those identified by the authors as responsible for turbulence modulation. The only consistent and exhaustive study of a given triplet was completed by Elghobashi et al. (1994) who successively observed the separate influence of τ_p, α and d_p. However, the use of computational particles to represent several real particles ($M_r/M_c = 100$) can mimic the characteristics of an heterogeneous

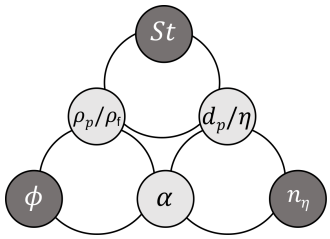

Figure 2: Controlling non-dimensional parameters for particles in turbulence.

disperse phase, though aiming at representing a highly-concentrated one (high "real" particle number density but low "computational" particle number density). As already noticed by Boivin et al. (1998), neither simulations of Squires and Eaton (1990); Elghobashi et al. (1994) nor their own calculations met the condition of $n_\eta >> 1$, required for correspondence between computational and actual particles. Therefore, only "real" particles ($M_r/M_c = 1$) are used in our study.

Attempts to assess the importance of some dimensionless parameters on turbulence modification have been made. Gore and Crowe (1989) claimed that the ratio of particle diameter to a turbulent length scale provides an estimate of whether the turbulent intensity of the carrier phase will be increased or decreased. Kenning and Crowe (1997) introduced a criterion based on a hybrid length scale defined with the dissipation length scale of the single-phase flow and average interparticle spacing. Tanaka and Eaton (2008) introduced a new dimensionless parameter Pa, the particle momentum number, involving the Stokes number, the ratio of particle and fluid densities, the Reynolds number, the ratio of particle diameter to a flow length scale. However, there is no general consensus on a single parameter responsible or not for the modulation of turbulence and their respective conclusions were sometimes contradictory: Tanaka and Eaton (2008) claimed that the Stokes number does not control turbulence modification whereas most of the other studies highlight its role. It thus seems clear that a single parameter is not sufficient in order to characterize the physics of such flows and we need to identify the ones to be considered.

Our choice of description for the disperse phase is represented by the darkest triplet

Figures	$\mathrm{St}(t_{inj})$	ϕ	n_η
Fig. 8 to 14, 18	$[0.3, 0.6, 1.2, 2.4, 4.8]$	$[0.1, 0.2, 0.3]$	$[0.07, 0.7, 7]$
Fig. 7, 15	$[0.6, 2.4]$	$[0.1, 0.2, 0.3]$	$[0.07, 0.17, 0.7, 1.7, 7, 17]$
Fig. 3, 16, 19, 20	0.6	0.001	$8.4 \times 2^j, j = -15, ..., 0$
Fig. 4	$[0.3, 1.2, 4.8]$	0	$[0.07, 0.7, 7]$

Table 3: Set of parameters for particles.

in Fig. 2. The choice of these three parameters was made in view of the proposed form of the interaction term. Indeed, in Eq. 9, mass loading is a factor as well as the inverse of the relaxation time of the particles. We therefore naturally wanted to be able to study the influence of each of these terms in modifying turbulence.

For the description of the system, we see in Fig. 2 that the third parameter can be the volume fraction, the particle diameter or the particle number density. From a modeling point of view, we have already seen that the number of particles plays a role in the description of the disperse phase in single-phase flows (Vié et al., 2016). We will see through this work that at fixed Stokes number and mass loading, particle distribution in space is essential to quantify the impact on the carrier phase.

In some of previous works such as those of Druzhinin and Elghobashi (1999) or Druzhinin (2001), particle field has been considered as perfectly homogeneous when $\mathrm{St} << 1$. This assumption was justified by considering that in the case of microparticles the preferential concentration is negligible. However, if particle number density is not large enough, the disperse phase cannot be considered as homogeneous even though the distribution of particles is uniform in the domain. One of the aim of the present work is to give a criterion on particle number density to determine what is the appropriate mean particle number density to consider the two-way exchanges as independent of this parameter.

In the present work, we apply direct numerical simulations to investigate turbulence modulation by inertial particles in decaying isotropic turbulence. Parameters of the

disperse phase were successively varied to provide data on modulation of turbulence features and energy spectra according to Table 3. In order to cover the entire parameters space, the exhaustive study of the three selected parameters is carried out according to the parameter values in the first line of Table 3. To emphasize the role played by the particle number density parameter, another set of simulations is performed, with a very large range of values for n_η. To satisfy the assumptions of sub-Kolmogorov particles and dilute regime, the mass fraction is set at a sufficiently low value $\phi = 0.001$.

3. Defining a measure of disperse phase heterogeneity

In turbulent flows, preferential concentration of particles is a major aspect that can strongly lead the physics (see Capecelatro and Desjardins (2015) for example). In the literature, several methods have been proposed to measure preferential concentration, and an exhaustive review is proposed by Monchaux et al. (2012). However, preferential concentration is not the only source of phase heterogeneity. Actually, when particle concentration is not high enough, the particulate phase cannot be seen as a continuum, and must therefore be considered as a set of individual particles, and this can have an impact on the form of the coupling (see for instance Zamansky et al. (2016)). This introduces an additional level of heterogeneity. Here we thus define the heterogeneity of the disperse phase as the combination of the preferential concentration, consequence of the interactions between particles and turbulence, and the lack of continuum, consequence of large particle interspace. In the following, we propose methods that permit to separate both sources, and we also propose a way to identify isolated particles.

3.1. Measurement of preferential concentration

A classical tool to quantify preferential concentration is the PDF of particle number density based on box counting, which depends on the box size, as demonstrated by Monchaux et al. (2012) and Hogan and Cuzzi (2001). Let us define $\mathcal{B}$ a set of N_b boxes and N_{pb}^b the number of particles in the box b. We introduce N_p the total number of particles in the domain. A possible index to quantify the preferential concentration is the normalized variance of the discrete number density field: $G(N_p, N_b) =$

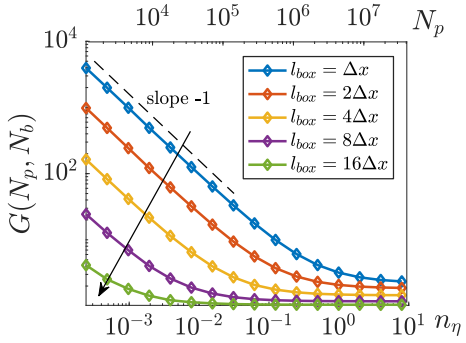

Figure 3: Evolution of preferential concentration with particle number density for different box sizes (the arrow shows the increase in box size). Fixed $\mathrm{St}(t_{inj}) = 0.6$ and $\phi = 0.001$ at $t_f = 6$.

$\frac{N_b}{N_p^2}\sum_{b\in\mathcal{B}}(N_{pb}^b)^2$. We provide a probabilistic analysis of the box counting measure in Appendix B: for one-way coupled simulations, it is possible to detail the asymptotic behavior of the measure. For two-way coupled simulations, we observe in Fig. 3 similar behaviors: linear slope for very low n_η and convergence with increasing particle number densities.

Fig. 3 not only confirms the dependency of the measure with the box size, but also highlights its dependency on the total number of particle N_p (or the particle number density n_η). For a given box size, the normalized variance appears to converge when increasing the number of particles. For sufficiently high particle number densities, the statistical sampling becomes redundant and saturated and increasing the number of particles does not add any information in the measure. Moreover, the threshold of convergence depends on the box size: smaller boxes require a higher particle number density to be completely sampled.

Another solution proposed in the literature is the use of Voronoï diagrams based on the Lagrangian point-particle cloud. The local particle concentration is the inverse of the volume of Voronoï cells v and unlike other segregation calculation methods such as box counting, they do not depend on the size of the box arbitrarily chosen. A direct measure for the preferential concentration is the standard deviation of Voronoï volume distributions: when clusters and vacuum regions are formed, the tails of the

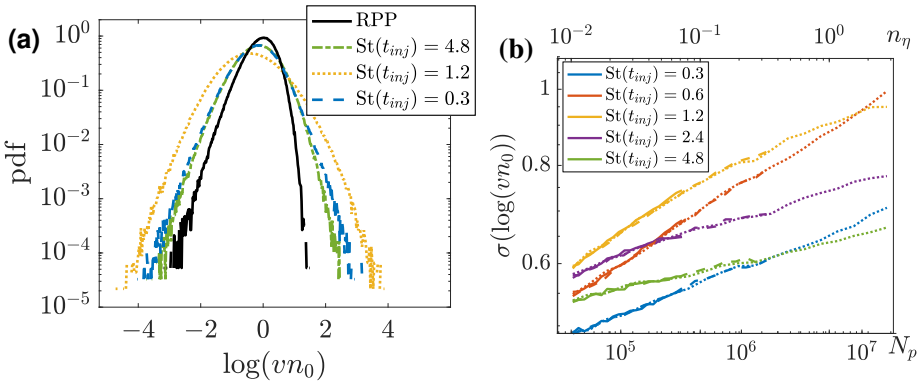

Figure 4: (a) PDF of normalized Voronoï volumes at $t_f = 6$. (b) Evolution of the standard deviation of the PDF with the number of particles in simulations, for successive sub-sampling in post-processing. Dotted lines (·····) : $n_\eta = 3.3$, dashed lines (- - -): $n_\eta = 0.33$ and solid lines (——): $n_\eta = 0.07$.

distributions are enhanced and the standard deviation increases.

Figure 4(a) shows the distribution of the normalized Voronoï volumes normalized by the average particle density[1], introduced by Monchaux et al. (2010). Three one-way coupled simulations are compared with different Stokes numbers and particle number densities at final time. Figure 4(a) also shows the distribution generated by a Random Poisson Process (RPP), which corresponds to the perfectly homogeneous case. For all three cases, the standard deviation is greater than for the Random Poisson Process, and it is maximal for a Stokes number close to unity, when the highest preferential concentration occurs.

In Fig. 4(b), we show the standard deviation of the Voronoï volume distribution $\sigma(\log(vn_0))$ for three original simulations with different particle number densities: $n_\eta = 0.07, 0.33, 3.3$, respectively the full, dashed and dotted lines. Similar to the box counting method, this measure also depends on the particle number density, and thus does not differentiate the source of heterogeneity between preferential concentra-

[1]We recall that the average particle density is independent of the spatial organization of particles.

tion and the lack of continuum. Such bias has already been studied by Monchaux (2012) who suggested to artificially sub-sample highly concentrated simulations in post-processing. Particles are randomly chosen and removed from the original data set. Sub-sampled simulations exhibit the same $\sigma(\log(vn_0))$ behavior for one-way simulations in Fig. 4(b). This is expected because the carrier phase is identical for all three simulations (one-way coupling) and the sub-sampling process before or after running the simulation leads to the same particulate field. In order to compare preferential concentration of particles between simulations with different number of particles, we apply the sub-sampling procedure to each simulation up to a number of particles of reference $N_p = 10^5$ (corresponding to $n_\eta = 0.02$). Note that this sub-sampling procedure was also used by Monchaux and Dejoan (2017).

To summarize, we compare the different measures of preferential concentration introduced above in Fig. 5(a), for several Stokes numbers. The box counting method based on the smallest boxes ($l_{box} = \Delta x$) reveals a strong statistical bias that can masks the preferential concentration of particles for very low particle number densities: the Stokes number dependency is not evident for the dotted curve in Fig. 5(a). This is corrected in the measure introduced by Monchaux, plotted in red in Fig. 5(b). Even for very low particle number densities, the Voronoï diagrams are well defined and the shape of the correct dependency on Stokes number is captured. However, there is still the statistical bias due to the mean particle number density. The black lines represents the unbiased measure after sub-sampling. The scaling of those black curves is consistent with the fact that the the Stokes number rules the preferential concentration, and that the only difference between the red curves is due to the additional sampling. Note that the value of the depleted measure still contains the effect of particle number density because it depends on the reference n_η chosen, but it is now independent of the particle number density of the original simulation. This quantifies the tendency for particles to gather in specific regions of the fluid.

3.2. Identification of isolated particles

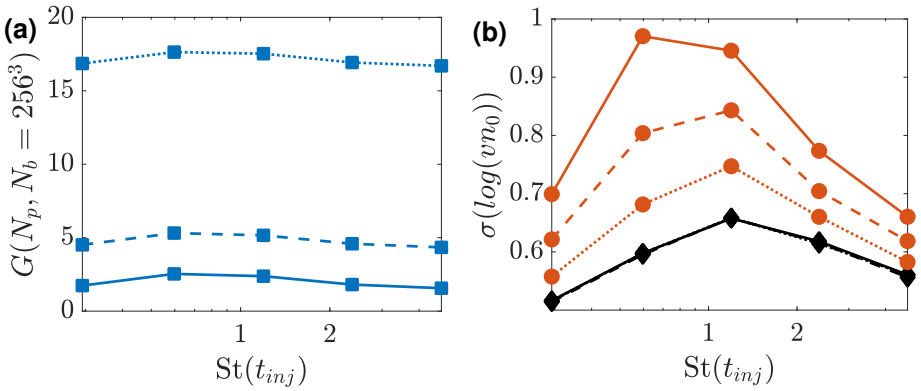

Figure 5: Comparison of preferential concentration for one-way coupled simulations. Dotted lines (·····) : $n_\eta = 0.07$, dashed lines (- - -): $n_\eta = 0.33$ and solid lines (——): $n_\eta = 3.3$. (a) Normalized variance of the number density field with box counting method; (b) Standard deviation of normalized Voronoï PDF before (red lines) and after (black lines) sub-sampling in post-processing.

Several works are interested in the identification of clusters with the Voronoï tesselation. For example, Monchaux et al. (2010) suggested a methodology to identify clusters as a connected set of low Voronoï volumes. This was used for instance by Zamansky et al. (2016) and improved by Baker et al. (2017). However, we seek here to identify isolated particles, which do not form a complementary set to clusters.

Voronoï cells produce a partition of the domain and thus, even in a regime where all particles are visibly part of a well-converged cluster as in the schematic example of Fig. 6, the cells of particles located at the border of the high density area will include the vacuum domain separating the other clusters. From the definition proposed by Monchaux et al. (2010), those specific particles are therefore not part of any clusters. However, we would like to include them in the cluster given that they are located in the high-density area. On the other hand, we would like to identify if particles are completely isolated from a cluster, and Voronoï volumes fails to provide this information because a large cell volume does not necessarily mean that the associated particle is in a void region. This is why we are considering a different distribution than the Voronoï volumes to avoid this eventuality.

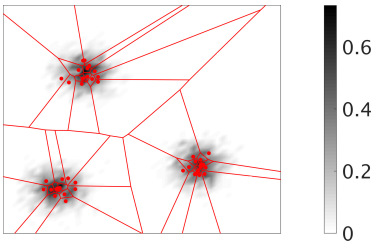

Figure 6: 2D Voronoï cells (red polygons) associated to particles (red points) superimposed with particle number density field (grey scale).

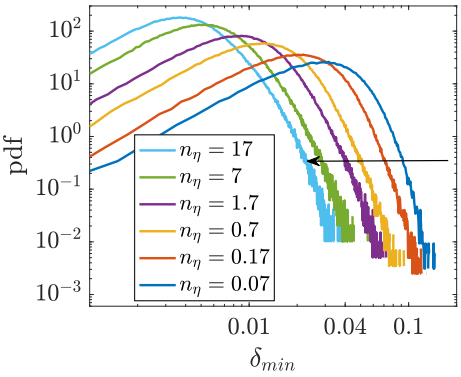

Figure 7: Probability density function of minimum interparticle distance for simulation with $\mathrm{St}(t_{inj}) = 0.6$ and $\phi = 0.3$ at $t_f = 6$. In our simulations, with the PSI-Cell approach, $2\delta_i = 2\Delta x = 0.04$.

Let us introduce the minimum interparticle distance δ_{min}, defined for each particle as the distance between the particle and its closest neighbor. Thus, even for particles on the boundary of a cluster, the minimum distance is small enough to consider that those particles belong to it, while the Voronoï criterion reflects the fact that they belong a vacuum region. The distributions of minimum interparticle distances is given in Fig. 7 for several particle number densities. Naturally, an increase in the particle number density results in a shift of the distribution towards lower values of interparticle distances.

3.3. Summary of proposed measures

We have introduced several measure of particle concentration. We have verified that the box counting measure of segregation converges with the number of particles (see Appendix B), and that particle preferential concentration can be compared between simulations with different number densities using the method of sub-sampling and volume Voronoï PDF. We will therefore use the box counting method to estimate the convergence of exchanges between particles and fluids at a given scale, and the volume Voronoï PDF will be helpful to compare particle preferential concentration in two-way coupled simulations in section 4.3.1. The minimum interparticle distance gives another characterization of the heterogeneity of the particulate phase, by allowing to identify isolated particles with large interparticle distances.

4. Results

An overview of the evolution of statistical quantities and spectra is presented in this section according to the three parameters St, ϕ and n_η. The results already observed in the literature for the influence of Stokes number and mass loading are retrieved. Focus is on the role played by the particle number density, and the importance of taking it into consideration for a heterogeneous disperse phase.

4.1. Two-way interaction energy rate

Despite the lack of consensus on a unique criterion for turbulence modulation by particles, the Stokes number has often been identified as one of the key parameters. For instance, Elghobashi (1994) provided a diagram showing the regimes of production or dissipation of turbulence by particles according to the Stokes number based on Kolmogorov time scale. Ferrante and Elghobashi (2003) also identified a critical Stokes number (based on the Kolmogorov time scale at injection time) for which particles do not change the total energy of the carrier phase (thereby named "ghosts particles"). Figure 8 shows similar results: the Stokes number does play a role in the modulation of the kinetic energy of the fluid, with a tendency to slow down the rate of energy decrease for low Stokes numbers, and to increase it for more inertial particles. The

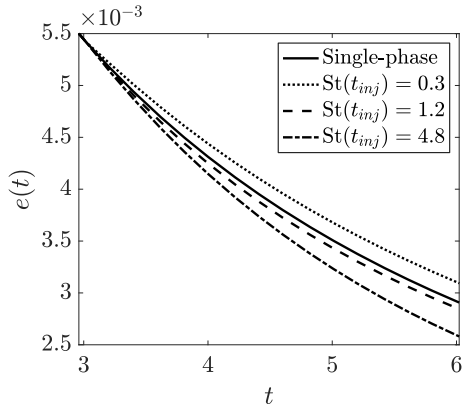

Figure 8: Turbulent kinetic energy temporal evolution for $\phi = 0.3$ and $n_\eta = 0.7$ from injection time $t_{inj} = 3$ to final time $t_f = 6$.

evolution equation of this decay rate (Eq. 9) is related to the dissipation term $-\varepsilon(t)$, to which is added the energy rate of change due to particle drag force $\psi_p(t)$.

Figure 9 describes the evolution of the two components of the decay rate: the fluid-particle coupling energy rate (Fig. 9(a)) and the dissipation rate (Fig. 9(b)) at a given time $t_f = 6$ and as a function of the final Stokes number. Both are normalized by the total energy budget of the carrier phase $e(t_f)$ and plotted with the same amplitude of y-axis in order to compare their relative magnitude.

The two-way interaction energy rate ψ_p depends on the velocity difference between the particle and its surrounding fluid, whereas ε depends on the strain rate only involving fluid gradients. Therefore, the only term accounting for the transfer of energy between the two phases is ψ_p as opposed to the modulation of ε which is the consequence of the propagation of the fluid perturbation around each particle. The two energy rates have very similar behaviors, and this correspondence is highlighted in Fig. 10 which groups the fluid dissipation values according to those of the fluid-particle exchange term. We believe that this strong correlation is a consequence of the fact that the dissipation rate is somehow a measure of the velocity gradients. As particle source term implies a perturbation of the velocity field, any modification due to particles leads to an immediate modification of the dissipation rate, in a strongly correlated manner.

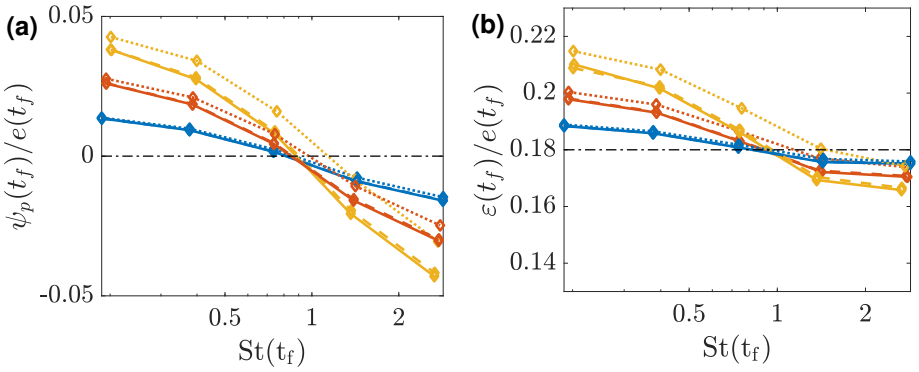

Figure 9: (a) Normalized fluid-particle exchange energy rate. (b) Normalized dissipation rate versus Stokes number at time $t_f = 6$. Lines blue: $\phi = 0.1$, red: $\phi = 0.2$, yellow: $\phi = 0.3$, ——: $n_\eta = 7$, - - -: $n_\eta = 0.7$, ·····: $n_\eta = 0.07$. The black dash-dotted line stands for the single-phase flow.

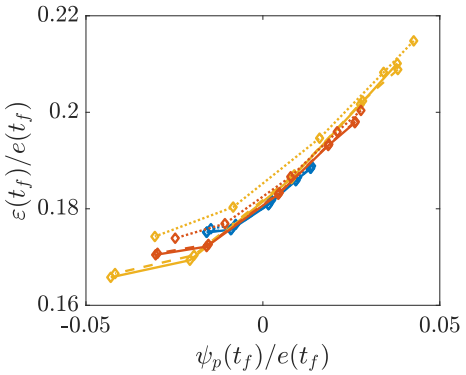

Figure 10: Normalized dissipation rate ε/e as a function of ψ_p/e. at time $t_f = 6$. Lines blue: $\phi = 0.1$, red: $\phi = 0.2$, yellow: $\phi = 0.3$, ——: $n_\eta = 7$, - - -: $n_\eta = 0.7$, ·····: $n_\eta = 0.07$. .

The reader can refer to the work of Ferrante and Elghobashi (2003), who gave a comprehensive analysis of the effect of particles on the dissipation ε by considering their impact on the vorticity field. The comparison of Figs. 9(a) and (b) shows that the magnitude of the change in dissipation ($(\varepsilon_{two-way} - \varepsilon_{one-way})/e$) is always smaller than the normalized source term ψ_p/e. Therefore, we will mainly focus on the two-way interaction energy rate and consider the dissipation as a consequence of this term.

We measure a change in the sign of ψ_p around Stokes number close to unity[2] in Fig. 9(a). In the case of $\mathrm{St} < 1$, the fluid-particle coupling energy rate ψ_p is positive, because the fluid-particle correlation along the particles paths $\langle u_{f,i}(\mathbf{x},t)\tilde{v}_{p,i}(\mathbf{x},t)\rangle$ is larger than the autocorrelation of the fluid $\langle u_{f,i}(\mathbf{x},t)\tilde{u}_{f@p,i}(\mathbf{x},t)\rangle$ (Ferrante and Elghobashi, 2003). With the inverse coupling, particle energy is given to the fluid resulting in an attenuation of the energy decay rate.

For Stokes numbers close to unity, particles are ejected from the large-vorticity cores but remain in their periphery. Even though fluid-particle energy rate is close to zero, the concentration of particles in those peripheric areas of vortices increases the dissipation.

Conversely, when the inertia of the particles increases, the fluid-particle coupling energy rate becomes negative due to a decorrelation between the velocities of the fluid and the particles. Inertial particles escape from their initial vortices and "cross" the trajectories of fluid points. Accordingly, ψ_p becomes negative and thus enhances the decay rate of turbulent kinetic energy.

In the scalar limit (for microparticles, i.e. $\mathrm{St} << 1$), the particle distribution is relatively uniform and particles behave like fluid-tracers. They are not ejected from the vortex cores and they retain their kinetic energy longer than the surrounding fluid. This is called "dusty gas", a phenomenon already described by Saffman (1962) and quantified analytically by Druzhinin (2001). The zeroth-order solution of the two-way

[2]The Stokes number calculated in our study is based on Kolmogorov scale at the measuring time $\tau_k = \sqrt{\nu_f/\varepsilon(t_f)}$, and not the injection time as it is defined by Ferrante and Elghobashi (2003)

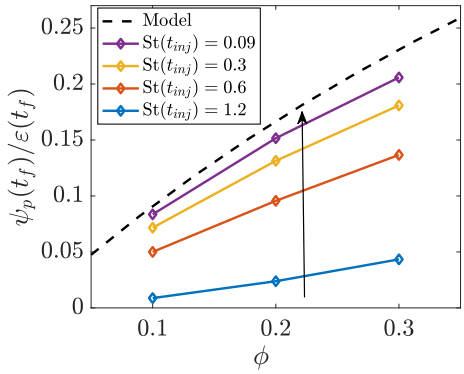

Figure 11: Fluid-particle coupling energy rate normalized by dissipation rate as a function of mass loading at $t_f = 6$. The arrow shows the decrease in Stokes number. The dotted line is the asymptotic limit analytically predicted.

coupling source term is in the form:

$$\psi_p(t) = \frac{\phi}{1+\phi}\varepsilon(t) + O(St) \tag{12}$$

This asymptotic behavior is retrieved in Fig. 11.

As expected, an increase in mass loading produces a more significant fluid-particle coupling term. Figure 12(a) suggests that a normalization by ϕ yields a scaling independent of mass loading. Thus, at high Stokes numbers, an increase in mass loading enhances the suppression of kinetic energy. On the contrary, at low Stokes numbers, ψ_p remains positive, and its absolute value increases, which slows down the natural decrease in the turbulent kinetic energy of the fluid. The particles with low Stokes number follow the fluid particles and thus uniformly charge the vortices, which therefore retain their vorticity longer. However this scaling is verified here for a very high particle number density $n_\eta = 7$ and we show in Fig. 12(b) that the behavior is not that simple for heterogeneous particle phases.

Figure 12(b), which shows the evolution of the normalized fluid-particle energy rate as a function of the particle number density, confirms that an heterogeneous disperse phase enhances the fluid-particle exchange term contribution. For very high number of particles, the source term is almost proportional to mass loading (the normalized plots

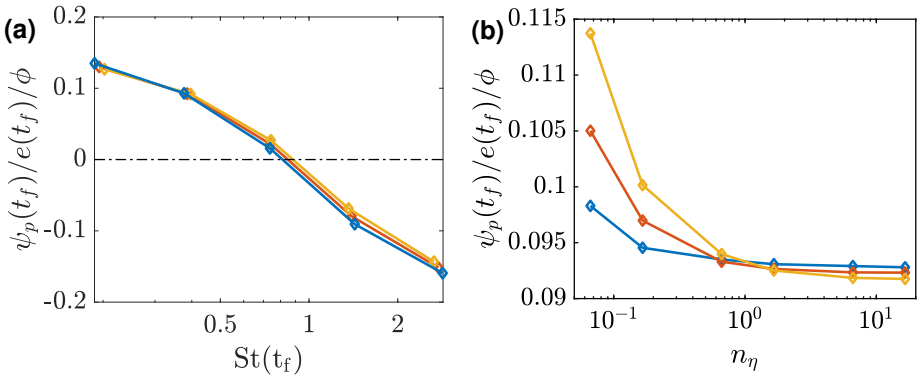

Figure 12: (a) Fluid-particle coupling energy rate normalized by mass loading for a fixed $n_\eta = 7$. (b) Two-way interaction energy rate normalized by total kinetic energy and mass loading at $t_f = 6$ with fixed $\mathrm{St}(t_{inj}) = 0.6$. Lines blue: $\phi = 0.1$, red: $\phi = 0.2$, yellow: $\phi = 0.3$.

are almost overlapping). However, for lower number of particles, the normalized two-way interaction term is stronger for high mass loadings than for low ϕ. For one-way coupled simulations, at fixed St, the dynamics of the particles is identical and thus the (hypothetical) two-way interaction term is strictly linear with the mass loading. For two-way coupled flows, the velocity of the fluid is locally modified by particles, thus changing the velocity correlations in the two-way interaction term. Even though the mass loading is in factor in the expression of ψ_p (see Eq. 9), the non-linear dependency of velocity correlations yields this non-overlapping of the curves. This figure precisely highlights the role played by particle number density in momentum exchanges between particle and carrier phases. The asymptotic behavior of the exchange term at very high particle number densities is reminiscent of the dependency of the box counting method with particle number density and is further developed in Appendix C.

4.2. Spectral space analysis of two-way coupling energy rate

The consequence on the coupling can be further examined by taking the evolution of the energy and forcing spectra. As already observed by Ferrante and Elghobashi (2003), even if the change in the total energy budget is not affected by the presence of small particles (in the case of ghost particles), it does not necessarily imply that the distribution of this energy in the different scales is uniformly zero.

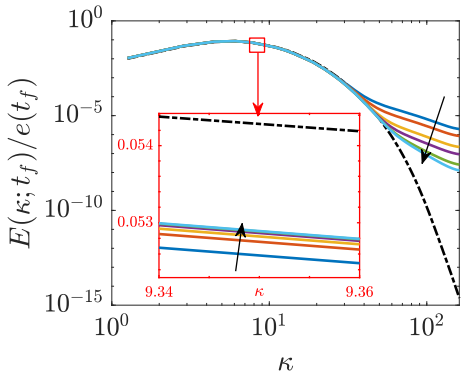

Figure 13: Normalized Energy spectrum $E(\kappa)/e$ at $t_f = 6$ for $\phi = 0.3$ and $\mathrm{St}(t_{inj}) = 2.4$. The arrows show the increase in the particle number density following this order: $n_\eta = 0.07, 0.17, 0.7, 1.7, 7, 17$. The dash-dotted line stands for the single-phase flow spectrum. The inset is a zoom on small wavenumbers.

In Fig. 13, the turbulence spectrum is plotted at time $t_f = 6$ for cases without particles, and in the two-way coupled cases for a fixed mass loading and Stokes number $St(t_{inj})$, and six different values of mean particle number densities n_η. The presence of particles enhances the energy at small scales while decreasing the energy at large scales, the overall turbulent kinetic energy being reduced because of the promoted turbulent dissipation. Furthermore, as the particle number density is increased, the spectrum tends to a limit one which corresponds to the highly-concentrated regime, as already discussed in Sec. 4.1 and in Appendix C.

The fluid-particle interaction spectrum has been extensively studied in the literature (Ferrante and Elghobashi, 2003; Fröhlich et al., 2018; Mallouppas et al., 2017; Abdelsamie and Lee, 2012; Druzhinin, 2001). In particular, Ferrante and Elghobashi (2003) compared $\Psi_p(\kappa)$ for different Stokes number and found similar results. Figure 14(a) shows that for particles with small Stokes number (microparticles), $\Psi_p(\kappa)$ is positive at almost all wavenumbers and thus produces a positive contribution to the decay rate $\partial E(\kappa)/\partial t$. On the other hand, the term is negative at almost all wavenumbers for larger Stokes numbers. For intermediate and large Stokes numbers, $\Psi_p(\kappa)$ remains positive for large κ while a negative peak appears in the spectrum for small κ.

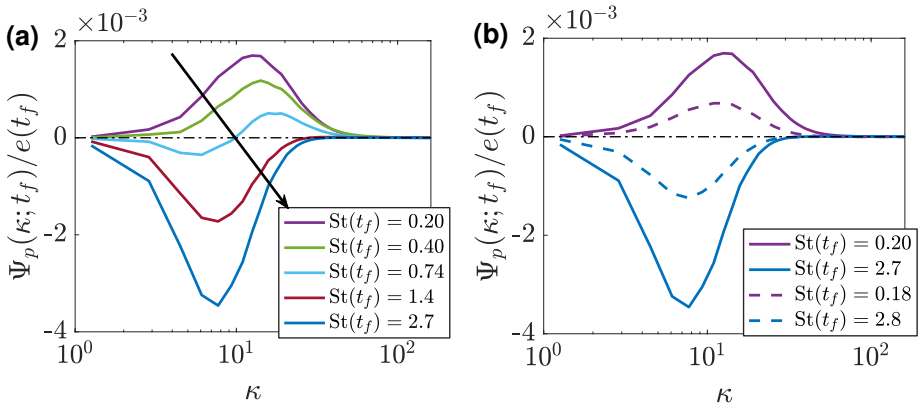

Figure 14: Normalized two-way interaction spectra $\Psi_p(\kappa)/e$ at $t_f = 6$ for $n_\eta = 7$. Influence of the Stokes number based on final time (a) and of mass loading (b). Solid lines (——): $\phi = 0.3$, dashed lines (- - -): $\phi = 0.1$

Figure 14(b) shows the spectral fluid-particle interaction for two different Stokes numbers and two different mass loading. As mentioned in section 4.1, the scaling between spectra with same Stokes number but different mass loading is close to the ratio of mass loading, but because of the non-linearity, we do not expect such scaling for higher mass loading.

Previous results show that a low particle number density results in an increase in the fluid-particle interaction energy rate $\psi_p(t)$, especially when the mass loading is high. Let us study the spectrum of this exchange term to identify at what scales the interactions between particles and fluid are located and how the distribution of mass loading can modify the fluid energy. We can see in Figs. 15(a) and 15(b) that a heterogeneous disperse phase ($n_\eta = 0.07$) systematically produces a larger $\Psi_p(\kappa)$ at small scales than a highly-concentrated one ($n_\eta = 17$). At large scales however, a heterogenous disperse phase reduces the two-way interaction contribution compared to higher particle number densities simulations.

We observe that the two-way interaction spectra are positive at the largest wavenumbers, even for large Stokes numbers (Fig. 14(b)). The feedback force in the momentum equation always results in a local alignment of fluid velocity around a particle with the

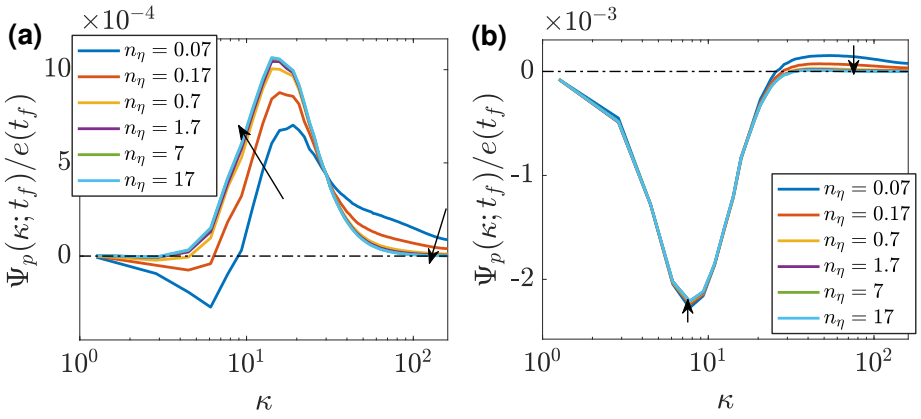

Figure 15: Spectral fluid-particle interaction plotted for different particle number densities n_η and fixed $\phi = 0.3$. (a) $\mathrm{St}(t_{inj}) = 0.60$; (b) $\mathrm{St}(t_{inj}) = 2.4$

particle velocity. The intensity of the feedback modulates this tendency to alignment. It is more obvious for low Stokes number, but it can also become important at high Stokes number and large mass loading.

4.3. Particle field heterogeneity

For a physical intuition of the interpretation of the spectra in section 4.2, the spatial distribution of the corresponding fields before the Fourier transform can be examined. Figure 16 compares the spatial distribution of the local two-way interaction energy rate $\widetilde{\psi}_p(\mathbf{x}, t) = \mathbf{u}_f(\mathbf{x}, t)\mathbf{f}(\mathbf{x}, t)/\rho_f$, with superimposed particles in a part of the flow domain at time $t = 6$. Particles parameters were set to the same Stokes number $\mathrm{St} = 1$, and global mass loading $\phi = 0.001$, but different particle number densities. Figure 15(a) shows that each isolated particle produces a localized contribution to the two-way interaction term, and therefore the two-way interaction field is more heterogeneous than for the case with higher n_η, accordingly to the corresponding particle concentration field. By increasing the particle number density n_η without changing the total mass ϕ nor the behavior of each particle defined by St, see Fig. 15(b), each particle produces a smaller individual effect on the fluid. On the other hand, the collective effect of segregated particles results in a smoother and well-distributed two-way interaction field.

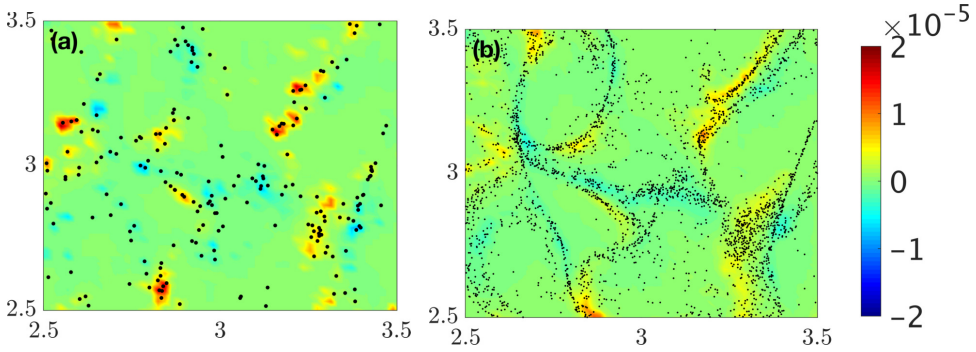

Figure 16: Distribution of two-way interaction energy rate $\widetilde{\psi}_p$ at $t = 6$ superimposed with particles parametrized by $\phi = 0.001$ and $\mathrm{St} = 1$. (a) $n_\eta = 0.12$; (b) $n_\eta = 2$

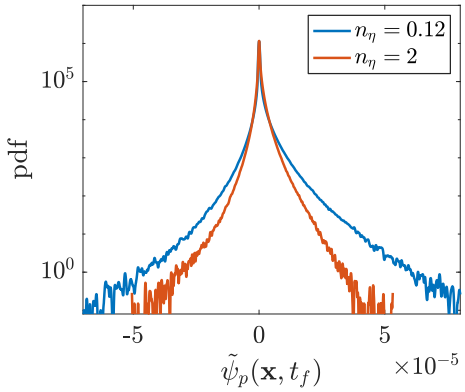

Figure 17: Distribution of the two-way interaction energy rate field $\widetilde{\psi}_p(\mathbf{x}, t)$ for the heterogeneous and highly-concentrated cases.

The probability distribution function of the corresponding spatial two-way interaction terms is plotted in fig. 17, and the reduction of the tails indicates a better distributed interaction term for highly-concentrated disperse phase.

4.3.1. Preferential concentration

Figure 18 shows the standard deviation of the normalized Voronoï volume distributions for the different configurations. As explained in section 3, the simulations were depleted in post-processing to equalize to the same number of particles in order to be able to compare them without statistical bias. The quasi-scaling of those curves is

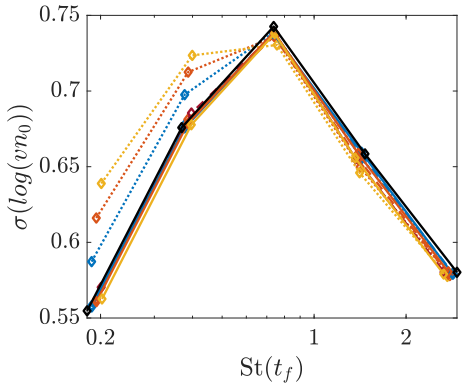

Figure 18: Comparison of preferential concentration for all simulations. Lines blue: $\phi = 0.1$, red: $\phi = 0.2$, yellow: $\phi = 0.3$, ——: $n_\eta = 7$, - - -: $n_\eta = 0.7$, ·····: $n_\eta = 0.07$. The black dash-dotted line stands for the single-phase flow.

consistent with the fact that the Stokes number based on up-to-date time governs the preferential concentration, revealing that the adaptation is faster than the decrease in energy. Only simulations with low particle number density and low Stokes number increase the preferential particle concentration effect. We can conclude that all the two-way coupling effects that we analyze in our simulations are not a consequence of a modification of the clustering.

4.3.2. Collective and isolated regimes

A single particle will interact and exchange energy with the surrounding fluid up to a characteristic length of δ_i, which is directly related to the size of the projection kernel[3]. The source term introduced in the fluid momentum equation is limited to the kernel envelope δ_i and we will consider that a particle is "isolated" if it is distant from others of more than $2\delta_i$ (the interaction zones of the two particles do not overlap). On the contrary, if two particles are closer than this length-scale, their corresponding source terms can overlap and these two particles form a "cluster".

Let us consider the two limit regimes where particles are either all isolated to each

[3]Using a trilinear projection, we verify that $\delta_i = \Delta x < \eta$

other, or all part of a cluster. Those two configurations correspond to the PDF of the minimal interparticle distance being respectively on the right or on the left side of the $2\delta_i = 2\Delta x$ boundary, see Fig. 7. These limit behaviors are indeed observed in Fig. 15: green and light blue distributions of Fig. 7 are on the left of $2\delta_i$ and produced in Fig. 15 almost identical spectra, because the particulate phase is already converged and increasing particle number density do not change the interaction spectrum anymore. However, for the other distributions, on the other side of the threshold, one can see in Fig. 15 that the spectra are strongly dependent on particle number density, especially at the smallest scales, the last ones to reach convergence.

Let us explained these limit behaviors. If particles are all isolated from each other, then the particles properties locally determine the amount of energy exchanged with the fluid and the global budget is a statistical average of all the exchanges. Thus, if we modify the properties of this particle, for example by decreasing the particle number density of the simulation while ensuring that we keep isolated particles, then the mass m_p of the single particle is now larger and the amount of energy transferred will be locally larger. In this regime, the two-way interaction spectrum is highly sensitive to particle number density, especially at the smallest scales of the fluid, where particles inject an energy almost proportional to their mass.

On the contrary, if every particle is part of a cluster, the force exerted by particles on the fluid can be assimilated to a continuous force on the cluster domain. By increasing particle number density but maintaining the mass loading, the total mass and therefore the energy contained in each cluster is unchanged. Therefore, the two-way interaction spectrum is unchanged, this collective regime leads to the two-way limit behavior observed for spectra.

This criterion is very restrictive, those two limit regimes are rarely reached and we propose in the next section an other approach to characterize the transition from the isolated to collective regime, scale by scale.

4.3.3. Scale by scale convergence

The two-way interaction spectrum indicates for each wavenumber the amount of energy introduced into the spectral equation. More precisely, each wave-number κ_l

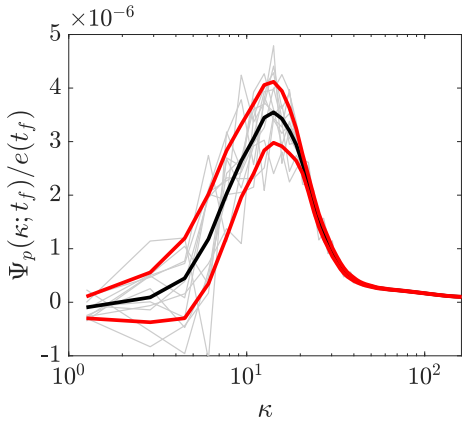

Figure 19: Normalized two-way interaction spectra $\Psi_p(\kappa)/e$ for 11 realizations of simulation with $n_\eta = 8.4 \times 2^{-14}$ (grey lines), the average spectrum $\bar{\Psi}_p(\kappa)/e$ (black solid line) and the standard deviation (red solid lines).

is associated to a physical size $l = \frac{2\pi}{\kappa_l}$. Thus, the term $\Psi_p(\kappa_l)$ specifies the average energy provided by the exchange term in boxes of size l contained in the domain.

Figure 19 shows several realizations (grey lines) of the interaction spectrum of a very heterogeneous disperse phase ($n_\eta = 8.4 \times 2^{-14} = 5.13 \times 10^{-4}$). The spectra are noisy at the largest scales due to a lack of samples available for the corresponding box sizes. We define a reconstructed spectrum, in black line, as the mean spectrum of all the realizations $\bar{\Psi}_p(\kappa) = \frac{1}{N_r} \sum_r \Psi_p(\kappa)$, where N_r is the number of realizations of the simulation (same parameters of the disperse phase and the gas phase but different initial particle distribution). The standard deviation is also plotted in red lines in Fig. 19. The variability between the different realizations is reduced at the smallest scales because one flow realization contains a sufficiently large sample of small eddies to ensure a meaningful sampling.

In the following, to only take into consideration the effect of a representative realization of a highly heterogeneous disperse phase, we consider the average spectrum associated with several realizations (black spectrum). We thus obtain smoothed spectra in Fig. 20(a) even for very low particle number densities.

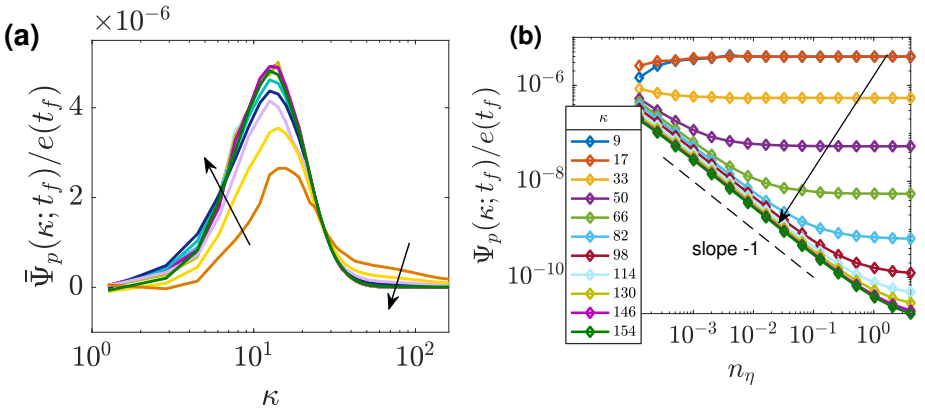

Figure 20: (a) Normalized two-way interaction spectra averaged between several realizations. (b) Evolution with n_η of the spectral values for different wavenumbers (the arrow indicates increasing wavenumbers).

In Fig. 20(b), we have plotted for several wavenumbers the evolution of the spectrum values at those scales when n_η increases.

For each graph in this figure, we observe two very distinct regimes: a first linear zone of slope -1 for low n_η, and a second zone for high n_η, in which the spectrum values are converged and are therefore no longer modified when the particle number density increases. Those regimes are respectively the isolated (linear) and collective (converged) regime introduced before. This scale-by-scale convergence can be correlated with the convergence of the segregation measure defined with bin counting of corresponding sizes in Fig. 3, and is also a consequence of the statistical sampling related to the scale in consideration: the large scales reach their asymptotic value for smaller n_η than small scales, because the number of particles per scale is larger.

Conclusion

An exhaustive study of the influence of the three parameters describing a monodispersed phase on isotropic homogeneous turbulence has been carried out. Classical results from the literature have been retrieved, in particular the global trends in energy

and spectral statistics with the Stokes number and mass loading. The study of the two-way coupling term here normalized by fluid kinetic energy and the use of a Stokes number based on instantaneous Kolmogorov scales have permitted to clearly identify two regimes: a first regime for $\mathrm{St} < 1$ in which particles reduce the decay of turbulent energy, and a second regime for $\mathrm{St} > 1$ in which particles enhance the decay.

Additionally to the existing literature, the present study has emphasized the influence of the particle number density on the coupling term. First, we ensured with a Voronoï analysis that the structure of turbulence is not strongly modified by the presence of particles: turbulence is sustained or dissipated but particle preferential concentration remains directly correlated to the updated Stokes number.

Numerical simulations have revealed that a highly heterogeneous particulate phase tends to increase the energy transmitted to the fluid. In particular, a spectral analysis showed that isolated particles inject energy at the finest scales while a continuous particulate phase no longer produces energy at these scales but rather at smaller wavenumbers. Those two regimes are reflected in the behavior of the energy spectra:

- At "small" scales, the spectrum is strongly dependent on particle number density and behave almost linearly with this parameter: the energy injected by particles is almost proportional to individual particle mass because particles are isolated regarding those specific scales.

- At "large" scales, the spectrum is no longer modified by the number of particles since the sampling is significant enough, all these scales necessarily contain a large number of particles.

- The limits for "small" and "large" scales depend on the mean particle number density.

- If the distribution of minimal interparticle distance is on the left side of η, the spectrum is completely converged: increasing particle number density does not modify the spectrum.

Furthermore, due to the high variability of the spectrum at large scales for low particle concentration, we have highlighted the necessity to construct statistics over several

flow-particles realizations.

This study therefore made it possible to determine precisely the conditions of partial or total convergence of the spectrum as a function of the particle number density, and more precisely of the distribution of interparticle distances.

As a conclusion, it must be noted that such regimes, whereas being intrinsically present in Lagrangian point-particle approaches, must be included and modeled when the carrier phase description is given by a reduced description such as Large Eddy Simulation. The use of adapted Lagrangian Stochastic models must be considered. For Eulerian approaches, even with a fully resolved carrier phase, accounting for heterogeneous regime requires new developments and closures at the kinetic level.

Acknowledgements

This work was supported by grants from Region Ile-de-France DIM MATHINNOV. It was granted access to the HPC resources of CINES under the allocation A0062B06172 made by GENCI (Grand Equipement National de Calcul Intensif), it was also performed using HPC resources from the mesocentre computing center of CentraleSupélec and Ecole Normale Supérieure Paris-Saclay supported by CNRS and Region Ile-de-France (http://mesocentre.centralesupelec.fr/). The authors thank R. Zamansky for fruitful discussions about coupling kernels, our thanks also extend to O. Simonin and E. Masi for the discussions on the measures of particle preferential concentration. Support from the French Agence Nationale de la Recherche in the MIMETYC project (grant ANR-17-CE22-0003) is also acknowledged.

Appendix A. Impact of the coupling kernel

The length-scale δ_i is the characteristic size of the domain of influence of a particle on the surrounding fluid. The numerical quantity associated is the size of the volume filtering kernel. Several works are dedicated to the determination of the parameter δ_i for finite size particles (see for instance Maxey and Patel (2001)), the objective being to ensure that the force distributions are completely contained within the interior of the particle. Capecelatro and Desjardins (2013) recommended $\delta_i \approx 3d_p$ but the minimal

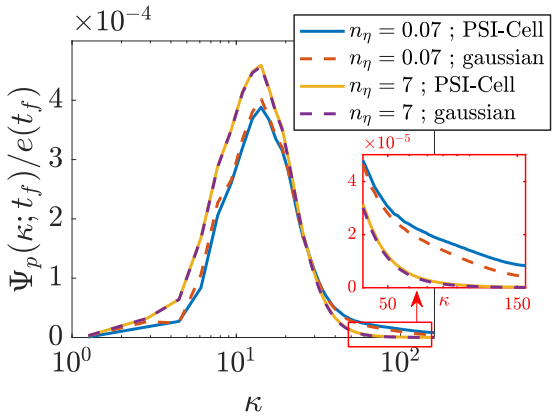

Figure A.21: Normalized two-way interaction spectrum with PSI-Cell (solid lines) and Gaussian (dashed lines) projections. Two different particle number densities are compared. The inset displays a zoom around the smallest scales.

value for δ_i is the grid spacing to avoid singularities in the carrier phase source term. The PSI-Cell approach implemented in Asphodele naturally yields $\delta_i = \Delta x$.

We also implemented another coupling kernel with a gaussian envelope of size $\sigma = \Delta x/2\sqrt{2ln(2)}$ such that the full width at half height of the kernel δ_i is equal to the grid spacing. This way, the effect of the particle is typically spread out over the 27 nearest cells. Results are compared with the trilinear projection kernel.

Thus, in Fig. A.21, the comparison of the interaction spectra obtained is consistent with the previous wavenumber analysis: for simulations with a large number of particles, statistical convergence is achieved at all scales and thus the kernel change has no impact on the interaction spectrum. On the other hand, at low particle number density, the small scales are less energetic with the Gaussian kernel which spread the energy of the particles at these scales over a larger range of cells. It should also be noted that large scales are then more energetic in this case, since the total interaction energy must be preserved.

Appendix B. Convergence of the box counting measure

Let us recall that N_{pb}^b is the random variable giving for each box $b \in \mathcal{B}$ the number of particles in the box. We define the box counting measure of particle preferential concentration as the normalized variance of the discrete particle number density field:

$$\begin{aligned} G(N_p, N_b) &= \frac{\frac{1}{N_b}\sum_{b\in\mathcal{B}}(N_{pb}^b)^2}{\left(\frac{1}{N_b}\sum_{b\in\mathcal{B}} N_{pb}^b\right)^2} \\ &= \frac{N_b}{N_p^2}\sum_{b\in\mathcal{B}}(N_{pb}^b)^2 \end{aligned}$$

The dependency of the measure with the total number of particles and the number of boxes is highlighted. One should also note that this measure is itself a random variable. In the following, we explain the asymptotic behaviors of the measure with the number of particles in the domain.

For very low values of N_p and samplings such that $\max_{b\in\mathcal{B}} N_{pb}^b \leq 1$, it is possible to detail the segregation. We have $G(N_p, N_b) = \frac{N_b}{N_p^2}\sum_{b\in\mathcal{B}}\delta_b$, where δ_b is 1 if a particle is in the box b, 0 otherwise. This yields: $G(N_p, N_b) \underset{N_p\to 0}{\sim} N_b N_p^{-1}$, hence the linear behavior with slope -1 of Fig. 3, and the shift between the different curves.

For very high values of N_p, we can assume that random variables N_{pb}^b are independent. It is known that N_{pb}^b follows a binomial distribution of parameters $B(N_p, p_b)$, where p_b is the probability for a particle to be in the box b (p_b is fixed and independent of N_p for one-way coupled simulations). The mean and variance of N_{pb}^b are respectively $N_p p_b$ and $N_p p_b(1-p_b)$). The expected value of the measure G is:

$$\begin{aligned} \mathbf{E}[G] &= \left(\frac{N_b}{N_p}\right)^2 \frac{1}{N_b}\sum_{b\in\mathcal{B}}\mathbf{E}[(N_{pb}^b)^2] \\ &= \left(\frac{N_b}{N_p}\right)^2 \frac{1}{N_b}\sum_{b\in\mathcal{B}} N_p p_b(1-p_b) + (N_p p_b)^2 \\ &= \frac{N_b}{N_p}\sum_{b\in\mathcal{B}} p_b(1 - p_b + N_p p_b) \\ \mathbf{E}[G] &\xrightarrow{N_p\to\infty} N_b \sum_{b\in\mathcal{B}} p_b^2 \end{aligned}$$

The particular case of uniform distribution, characterized by $p_b = p$ for all k yields a convergence towards 1.

We also verify that the variance of the measure tends to zeros when N_p tends to infinity :

$$\begin{aligned}\mathrm{Var}[G] &= \mathbf{E}[G^2] - \mathbf{E}[G]^2 \\ &= \Big(\frac{N_b}{N_p}\Big)^4 \Big\{\mathbf{E}[\langle (N_{pb}^b)^2\rangle_b^2] - \mathbf{E}[\langle (N_{pb}^b)^2\rangle_b]^2\Big\}\end{aligned}$$

The second term in the variance behaves like:

$$\begin{aligned}\Big(\frac{N_b}{N_p}\Big)^4 \mathbf{E}[\langle (N_{pb}^b)^2\rangle_b]^2 &= N_b^2 \Big(\sum_{b\in\mathcal{B}} p_b^2\Big)^2 + O(N_p^{-1}) \\ &= N_b^2 \sum_{i\in\mathcal{B}}\sum_{j\in\mathcal{B}} p_i^2 p_j^2 + O(N_p^{-1})\end{aligned}$$

The first term expands as:

$$\Big(\frac{N_b}{N_p}\Big)^4 \mathbf{E}[\langle (N_{pb}^b)^2\rangle_b^2] = \frac{N_b^2}{N_p^4} \sum_{i\in\mathcal{B}}\sum_{j\in\mathcal{B}} \mathbf{E}[(N_{pb}^i)^2 (N_{pb}^j)^2]$$

The random variables N_{pb}^b are independent, thus:

$$\begin{aligned}\text{for } i \neq j, \quad \mathbf{E}[(N_{pb}^i)^2 (N_{pb}^j)^2] &= \mathbf{E}[(N_{pb}^i)^2]\mathbf{E}[(N_{pb}^j)^2] \\ &= N_p^4 p_i^2 p_j^2 + O(N_p^3) \\ \text{for } i = j, \quad \mathbf{E}[(N_{pb}^i)^2 (N_{pb}^j)^2] &= \mathbf{E}[(N_{pb}^i)^4] \\ &= \sum_{k=0}^{4} \frac{N_p!}{(N_p-k)!} S(4,k) p_i^k \\ &= N_p^4 p_i^4 + O(N_p^3)\end{aligned}$$

where $S(n,k)$ are the Stirling numbers of the second kind. The first and second term therefore simplify and we have $\mathrm{Var}[G] = O(N_p^{-1})$. This explains the convergence of the measure for one-way coupled simulations.

Appendix C. Two-way interaction energy rate convergence

We show that the source terms in Fig. 12(b) converge towards an asymptotic limit value. It is assumed that convergence is based on the average volume of Voronoï cells

ϕ	p	$\psi_p(N_{p,max})$	ψ_p^∞
0.1	0.7219	0.0928	0.0931
0.2	1.1210	0.0923	0.0927
0.3	1.0050	0.0918	0.0926

Table C.4: Estimation of the converged values using Richardson's extrapolation.

i.e. $v(N_p) = L^3/N_p$. In order to evaluate the level of convergence in terms of particle number density, we apply a Richardson's extrapolation considering the parameter to be varied is not the mesh size, but the number of particle. We thus postulate

$$\psi_p(N_p) - \psi_p^\infty = Cv(N_p)^p$$

where $\psi_p(N_p)$ is the two-way interaction energy rate with N_p particles in the domain, ψ_p^∞ is the theoretical value of the quantity ψ_p at convergence, C is a constant, and p is an estimate of the order of convergence. If we are in the asymptotic regime, these two constants, C, p are fixed and we use the Richardson extrapolation to obtain the values of the constants as well as an estimate of the two-way interaction value at convergence. With three values of $\psi_p(N_p)$ taken with a constant ratio $r = 10$ between the $v(N_p)$, we estimate:

$$p = -\frac{1}{\ln(r)} \ln\Big(\frac{|\psi_p(r^2 N_p) - \psi_p(rN_p)|}{|\psi_p(rN_p) - \psi_p(N_p)|}\Big)$$

$$C = \frac{\psi_p(r^2 N_p) - \psi_p(rN_p)}{v(r^2 N_p)^p - v(rN_p)^p}$$

Values at convergence are listed in Table C.4. We observed that estimated converged value is very close to the value obtained with the maximum number of particles in our study.

References

Abdelsamie, A.H., Lee, C., 2012. Decaying versus stationary turbulence in particle-laden isotropic turbulence: Turbulence modulation mechanism. Physics of Fluids 24, 15106. doi:10.1063/1.3678332.

Baker, L., Frankel, A., Mani, A., Coletti, F., 2017. Coherent clusters of inertial particles in homogeneous turbulence. Journal of Fluid Mechanics 833, 364–398. doi:10.1017/jfm.2017.700.

Balachandar, S., Liu, K., Lakhote, M., 2019. Self-induced velocity correction for improved drag estimation in Euler–Lagrange point-particle simulations. Journal of Computational Physics 376, 160–185. doi:10.1016/j.jcp.2018.09.033.

Boivin, M., Simonin, O., Squires, K.D., 1998. Direct numerical simulation of turbulence modulation by particles in isotropic turbulence. Journal of Fluid Mechanics 375, 235–263.

Capecelatro, J., Desjardins, O., 2013. An Euler-Lagrange strategy for simulating particle-laden flows. Journal of Computational Physics 238, 1–31. doi:10.1016/j.jcp.2012.12.015.

Capecelatro, J., Desjardins, O., 2015. Mass Loading Effects on Turbulence Modulation by Particle Clustering in Dilute and Moderately Dilute Channel Flows. Journal of Fluids Engineering 137, 111102. doi:10.1115/1.4030644.

Capecelatro, J., Desjardins, O., Fox, R.O., 2015. On fluid-particle dynamics in fully developed cluster-induced turbulence. Journal of Fluid Mechanics 780, 578–635. doi:10.1017/jfm.2015.459.

Crowe, C.T., Sharma, M.P., Stock, D.E., 1977. The particle-source-in cell (PSI-CELL) model for gas-droplet flows. Journal of fluids engineering 99, 325–332.

Druzhinin, O.A., 2001. The influence of particle inertia on the two-way coupling and modification of isotropic turbulence by microparticles. Physics of Fluids 13, 3738–3755. doi:10.1063/1.1415735.

Druzhinin, O.A., Elghobashi, S., 1999. On the decay rate of isotropic turbulence laden with microparticles. Physics of Fluids 11, 602. doi:10.1063/1.869932.

Eaton, J.K., Fessler, J.R., 1994. Preferential concentration of particles by turbulence. International Journal of Multiphase Flow 20, 169–209. doi:10.1016/0301-9322(94)90072-8.

Elghobashi, S., 1994. On predicting particle-laden turbulent flows. Applied Scientific Research 52, 309–329. doi:10.1007/BF00936835.

Elghobashi, S., Truesdell, G.C., Elghobashi, S., 1994. On the two-way interaction between homogeneous turbulence and dispersed solid particles. II. Particle dispersion. Physics of Fluids A: Fluid Dynamics 6, 1790–1801. doi:10.1063/1.858854.

Ferrante, A., Elghobashi, S., 2003. On the physical mechanisms of two-way coupling in particle-laden isotropic turbulence. Physics of Fluids 15, 315–329. doi:10.1063/1.1532731.

Février, P., Simonin, O., Squires, K.D., 2005. Partitioning of particle velocities in gas-solid turbulent flows into a continuous field and a spatially uncorrelated random distribution: Theoretical formalism and numerical study. Journal of Fluid Mechanics 533, 1–46. doi:10.1017/S0022112005004088.

Fröhlich, K., Schneiders, L., Meinke, M., Schröder, W., 2018. Validation of Lagrangian two-way coupled point-particle models in large-eddy simulations. Flow, Turbulence and Combustion 101, 317–341. doi:10.1007/s10494-018-9933-3.

Gore, R.A., Crowe, C.T., 1989. Effect of particle size on modulating turbulent intensity. International Journal of Multiphase Flow doi:10.1016/0301-9322(89)90076-1.

Gualtieri, P., Picano, F., Sardina, G., Casciola, C.M., 2015. Exact regularized point particle method for multiphase flows in the two-way coupling regime. Journal of Fluid Mechanics 773, 520–561. doi:10.1017/jfm.2015.258, arXiv:1405.6969.

Hogan, R.C., Cuzzi, J.N., 2001. Stokes and Reynolds number dependence of preferential particle concentration in simulated three-dimensional turbulence. Physics of Fluids 13, 2938–2945. doi:10.1063/1.1399292.

Horwitz, J.A., Mani, A., 2016. Accurate calculation of Stokes drag for point-particle tracking in two-way coupled flows. Journal of Computational Physics 318, 85–109. doi:10.1016/j.jcp.2016.04.034.

Ireland, P.J., Desjardins, O., 2017. Improving particle drag predictions in Euler–Lagrange simulations with two-way coupling. Journal of Computational Physics 338, 405–430. doi:10.1016/j.jcp.2017.02.070.

Kenning, V.M., Crowe, C.T., 1997. On the effect of particles on carrier phase turbulence in gas-particle flows. International Journal of Multiphase Flow doi:10.1016/S0301-9322(96)00070-5.

Lele, S.K., 1992. Compact finite difference schemes with spectral-like resolution. Journal of computational physics 103, 16–42. doi:10.1016/0021-9991(92)90324-R.

Mallouppas, G., George, W.K., van Wachem, B.G.M., 2013. New forcing scheme to sustain particle-laden homogeneous and isotropic turbulence. Physics of Fluids 25, 83304. doi:10.1063/1.4818553.

Mallouppas, G., George, W.K., van Wachem, B.G.M., 2017. Dissipation and inter-scale transfer in fully coupled particle and fluid motions in homogeneous isotropic forced turbulence. International Journal of Heat and Fluid Flow 67, 74–85. doi:10.1016/j.ijheatfluidflow.2017.07.006.

Maxey, M.R., Patel, B.K., 2001. Localized force representations for particles sedimenting in Stokes flow. International Journal of Multiphase Flow 27, 1603–1626. doi:10.1016/S0301-9322(01)00014-3.

Maxey, M.R., Patel, B.K., Chang, E.J., Wang, L.P., 1997. Simulations of dispersed turbulent multiphase flow. Fluid Dynamics Research 20, 143–156. doi:https://doi.org/10.1016/S0169-5983(96)00042-1.

Monchaux, R., 2012. Measuring concentration with Voronoï diagrams: the study of possible biases. New Journal of Physics 14, 95013. doi:10.1088/1367-2630/14/9/095013.

Monchaux, R., Bourgoin, M., Cartellier, A., 2010. Preferential concentration of heavy particles: A Voronoï analysis. Physics of Fluids 22, 103304. doi:10.1063/1.3489987.

Monchaux, R., Bourgoin, M., Cartellier, A., 2012. Analyzing preferential concentration and clustering of inertial particles in turbulence. International Journal of Multiphase Flow 40, 1–18. doi:10.1016/j.ijmultiphaseflow.2011.12.001.

Monchaux, R., Dejoan, A., 2017. Settling velocity and preferential concentration of heavy particles under two-way coupling effects in homogeneous turbulence. Physical Review Fluids 2, 104302. doi:10.1103/PhysRevFluids.2.104302.

Poelma, C., Westerweel, J., Ooms, G., 2007. Particle-fluid interactions in grid-generated turbulence. Journal of Fluid Mechanics 589, 315–351. doi:10.1017/S0022112007007793.

Pope, S.B., 2000. Turbulent Flows. Cambridge university press. doi:10.1088/0957-0233/12/11/705.

Poustis, J.F.F., Senoner, J.M.M., Zuzio, D., Villedieu, P., 2019. Regularization of the Lagrangian point force approximation for deterministic discrete particle simulations. International Journal of Multiphase Flow 117, 138–152. doi:10.1016/j.ijmultiphaseflow.2019.04.021.

Reveillon, J., Demoulin, F.X., 2007. Effects of the preferential segregation of droplets on evaporation and turbulent mixing. Journal of Fluid Mechanics 583, 273–302. doi:10.1017/S0022112007006180.

Saffman, P.G., 1962. On the stability of laminar flow of a dusty gas. Journal of Fluid Mechanics 13, 120–128. doi:10.1017/S0022112062000555.

Squires, K.D., Eaton, J.K., 1990. Particle response and turbulence modification in isotropic turbulence. Physics of Fluids A: Fluid Dynamics 2, 1191–1203. doi:10.1063/1.857620.

Squires, K.D., Eaton, J.K., 1994. Effect of Selective Modification of Turbulence on Two-Equation Models for Particle-Laden Turbulent Flows. Journal of Fluids Engineering 116, 778. doi:10.1115/1.2911849.

Strutt, H.C., Tullis, S.W., Lightstone, M.F., 2011. Numerical methods for particle-laden DNS of homogeneous isotropic turbulence. Computers & Fluids 40, 210–220. doi:10.1016/j.compfluid.2010.09.003.

Sundaram, S., Collins, L.R., 1999. A numerical study of the modulation of isotropic turbulence by suspended particles. Journal of Fluid Mechanics 379, 105–143. doi:10.1017/S0022112098003073.

Tanaka, T., Eaton, J.K., 2008. Classification of turbulence modification by dispersed spheres using a novel dimensionless number. Physical Review Letters 101, 114502. doi:10.1103/PhysRevLett.101.114502.

Vié, A., Pouransari, H., Zamansky, R., Mani, A., 2016. Particle-laden flows forced by the disperse phase: Comparison between Lagrangian and Eulerian simulations. International Journal of Multiphase Flow 79, 144–158. doi:10.1016/j.ijmultiphaseflow.2015.10.010.

Zamansky, R., 2019. Lecture on Turbulent dispersed multiphase Flows, in: CISM Course on "Advances in Dispersed Multi-Phase Flows: from Measuring to Modeling", Udine, Italy.

Zamansky, R., Coletti, F., Massot, M., Mani, A., 2014. Radiation induces turbulence in particle-laden fluids. Physics of Fluids 26, 1–8. doi:10.1063/1.4890296.

Zamansky, R., Coletti, F., Massot, M., Mani, A., 2016. Turbulent thermal convection driven by heated inertial particles. Journal of Fluid Mechanics 809, 390–437. doi:10.1017/jfm.2016.630.